https://doi.org/10.1016/j.polymdegradstab.2019.03.002

Thermal, Crystalline and mechanical properties of Flame Retarded Poly(lactic acid) with a PBO-like small molecule - Phenylphosphonic Bis(2-aminobenzothiazole)

Benjamin Tawiah [a1], Bin Yu [a1], Anthony C. Y. Yuen [b], Richard K.K. Yuen [c], John H. Xin [a], Bin Fei [a*],

[a] Institute of Textiles and Clothing, Hong Kong Polytechnic University, Hong Kong, China

[b] School of Mechanical and Manufacturing Engineering, University of New South Wales, Sydney, NSW 2052, Australia

[c] Department of Civil and Architectural Engineering, City University of Hong Kong, Hong Kong, China

*Corresponding Author: Bin Fei

Tel: +852 27664795, Email: bin.fei@polyu.edu.hk

[1] These authors contributed equally (co-first author).

Abstract

Poly(lactic acid) (PLA) has received considerable attention due to its potential to replace the petrochemically derived plastics. However, its high flammability and the tendency to melt drip during combustion has restricted its applications in many areas. This manuscript reports the synthesis, characterization, and application of PBO-like small molecule additive flame retardant (FR) - phenylphosphonic bis(2-aminobenzothiazole) (P-ABZT) for bioplastic PLA. P-ABZT was incorporated into PLA by the combinatory solvent mixing and the compression molding approaches, and its FR, crystalline and mechanical properties were investigated. Fourier transform infrared (FTIR), ^{1}H, ^{13}C, and ^{31}P NMR confirmed the success of the synthetic process while thermogravimetric analysis (TGA) showed improved thermal stability and higher char yield after phosphorous was introduced. Cone calorimeter test demonstrated substantial reductions in peak heat release rate (PHRR ~ 50%), total heat released (THR ~ 37%), average effective heat of combustion (AEHC ~ 31%), peak CO and CO_2 produced (PCOP ~ 60.4 %, PCO_2P ~ 31 %) with just 3% P-ABZT loading. The limiting oxygen index (LOI) improved to 32.4% whilst a V-0 rating was attained in the UL-94 vertical burning test. Substantial reductions in pyrolysis gaseous products were obtained by P-ABZT/PLA composites compared to neat PLA in the TG-IR study. The Young's modulus, tensile strength, and elongation at break of PLA were not compromised with 1% P-

ABZT loading. SEM and Raman spectroscopy showed improved char yield and quality due to the condensed and gas phase inhibition by P-ABZT. The low FR loading coupled with the improved FR performance indicates that P-ABZT is an excellent and economical FR for PLA.

Keywords: Poly(lactic acid); flame retardant; phosphorous; cone calorimeter test; crystallization; mechanical properties; pyrolysis products.

Introduction

The interest in flame retardant (FR) poly(lactic acid) (PLA) has increased in recent years due to its versatility and biodegradability [1, 2]. With the continuous effort in research and development in recent years, different polylactide modifications have been engineered, making it widely applicable in many fields for different products [3-5]. Despite its broad applications and biodegradable properties, notable setbacks such as high flame flammability, severe melt dripping, and the release of toxic fumes remains a challenge.

Over the past decade, significant progress has been made on FR PLA, from the use of additives to intrinsic polymer modifications [6, 7]. The use of halogenated flame retardant (HFR) additives has over the years proven to be effective, but their adverse health and environmental effects far outweigh their merits, leading to their ban in several products [8]. The quest for environmentally benign alternatives to the halogen-free FRs has led to the discovery of other essential FR additives such as aluminum hydroxides, magnesium hydrate, phosphorus, 1D and 2D materials [6, 9-12], etc. The metal hydroxides (MHs) are the most readily available commercial FRs, but their efficiency is highly dependent on high loading of about 30 - 60 wt%, which usually affects the mechanical and crystalline properties of the polymer [6, 11].

Intumescent FRs and their synergies have also been investigated extensively, but like the MHs, they also require high loading for their efficiency to be fully realized [13-15].

The 1D and 2D fillers are mostly efficient when applied alone, modified or used synergistically with other traditionally-known FRs [11, 16, 17]. As a result, an efficient FR system made up of cobalt oxide-functionalized graphene composites was prepared to reduce the fire hazards of aliphatic polyesters[18]. Similarly, graphene and an ionic liquid containing phosphonium were melt-blended with PLA, and significant enhancement in flame retardancy was obtained [19]; meanwhile, the issue of high loading and economic viability remains in doubt [20]. Phosphorus FRs have received considerable attention lately due to their commercial significance [21, 22]. Given the interest in phosphorus FRs, Mauldin et al. synthesized and applied isosorbide-based polyphosphonate in PLA and achieved V-2 and V-0 ratings with 5 and 15 wt% FR loading respectively. However, an insignificant reduction in PHRR was attained, and the mechanical properties of the polymer were affected due to the high FR loading [23]. In a similar endeavor, Yu et al. investigated polysulfonyldiphenylene phenyl phosphonate FR at 10 wt% loading in PLA and reported improvement in the melt dripping with an LOI of 29.2% and a V-O rating but only a minimal reduction in PHRR was achieved, and the mechanical properties were hugely compromised [24]. In cases where low content P FRs are used, only slight improvement in PHRR and THR were achieved [25, 26].

To attain good FR performance at low loadings, the use of a phosphorous compound containing significant nitrogen content has been proposed [22, 27, 28]. Such FRs are deemed to have a potentially lower toxicological effect, higher thermal stability and are highly efficient at lower loadings [14]. Consequently, an improved FR performance can be achieved at a more economical loading with a less detrimental effect on the mechanical properties of the ensuing composite. Based on this supposition, phenylphosphonic di-benzothiazolyl imine-type tautomer was prepared and used as a co-curing agent for FR epoxy resin where a V-0 rating with and an LOI of 31.0% was achieved [29]. The benzothiazole

compounds have a unique chemical structure similar to polybenzoxazole (PBO) (inherent FR polymer) [30], hence the high FR efficiency. Meanwhile, the application of small molecule, PBO-like compound as additive FR for PLA has rarely been reported. The synthesized small molecule PBO-like compound has distinct FR properties due to the presence of phosphorus, nitrogen, sulfur and secondary amine groups in its backbone with no polar groups which can hydrolyze PLA prematurely during processing.

The objective of this manuscript is to synthesize a small molecule PBO-like FR additive for PLA and apply it via solvent mixing/compression molding approaches at low loading (3 wt% maximum) and evaluate its crystalline, thermal, FR, mechanical properties, and elucidate the possible FR mechanism.

2 Experimental

2.1 Materials

Poly(lactic acid) (Bioplus 6201D) was sourced from NatureWorks, 15305 Minnetonka Blvd., Minnetonka, USA. Phenylphosphonic dichloride (PPDCl) (90%) and Dimethyl sulfoxide-d6 (99.5% were purchased from Sigma Aldrich (Germany). 2-Aminobenzothiazole (ABZT) (97%, mp. 126-127 ^{o} C), triethylamine, anhydrous tetrahydrofuran (THF) (99.9%), acetone (99.9%), and chloroform (99.5%) were purchased from Acros organics (USA).

2.2 Synthesis of phenylphosphonic bis(2-aminobenzothiazole) (P-ABZT)

P-ABZT was synthesized according to scheme 1 similar to the literature [29] with significant modifications. Typically, a round-necked bottom flask equipped was set up in fume hood a humidity of RH 14%, and a temperature controller and magnetic stirrer after which 3 g (0.02mol) ABZT and 2.02 g (0.021 mol) triethylamine in 40 mL anhydrous THF was charged with at 0 - 5 ^{o}C for 1 h. Afterward, 1.95 mL PPDCl (0.01 mol) dissolved in 10 mL anhydrous THF was added dropwise. The reaction continued

for 6 h at 0 - 5 ^{o}C and then at room temperature for another 6 h for the precipitate to develop. The precipitated product was filtered and washed several times with THF and water to remove the unreacted monomers, and the triethylamine hydrochloride generated. The product was dried at 65 ^{o}C for 12 h, and P-ABZT with a product yield of 78%. The molecular weight was theoretically determined (MW. 423.4). ^{1}H NMR (400 MHz, DMSO-d6) δ = 7.79 (dd, J=41.7, 7.0, 3H), 8.09 – 7.35 (m, 3H), 8.09 – 7.46 (m, 2H), 8.12 – 7.45 (m, 2H), 7.30 (s, 1H), 7.23 – 6.79 (m, 2H), 3.11 (d, J=474.4, 21H). ^{13}C NMR (400 MHz, DMSO-d6) δ = 131.60, 131.28 130.68, 128.11, 126.61, 126.37, 125.99, 125.78, 123.17, 122.69, 122.46, ^{31}P NMR (400 MHz, DMSO-d6) δ = 12.25.

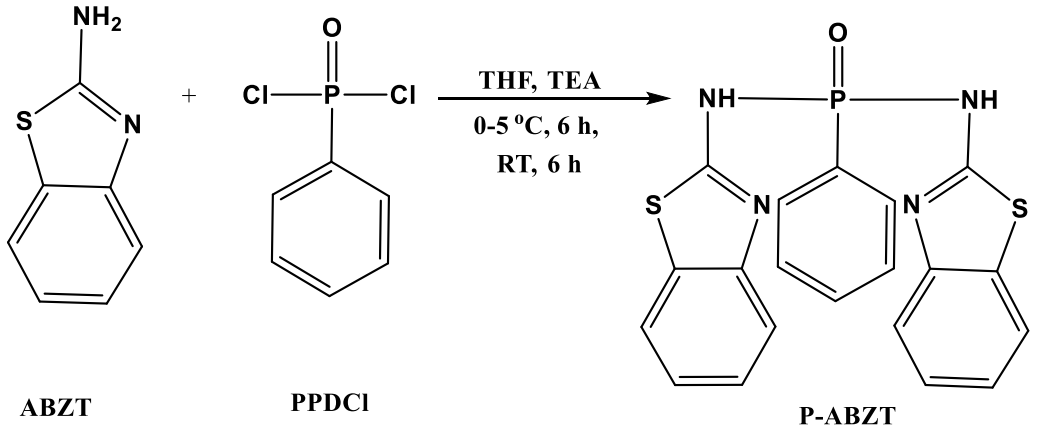

Scheme 1. Synthetic route of phenylphosphonic bis(2-aminobenzothiazole) (P-ABZT)

2.3Preparation of PLA/P-ABZT composites

PLA/P-ABZT composites were prepared by the solvent approach similar to the literature [31]. A predetermined quantity of P-ABZT (see Table S1) was dispersed in 30 mL chloroform and ultrasonicated for 30 min. A certain quantity of PLA (Table S1) was also dissolved in 300 mL chloroform with the aid of a mechanical stirrer at 700 r/min. The dispersed P-ABZT was mixed with the dissolved PLA and stirred for 2 h to obtain a homogenous PLA/P-ABZT composite. The temperature composite was increased to 50

^{o}C to allow some amount of solvent to evaporate. The PLA/P-ABZT composite was cast into a mold and dried in an oven at 60 ^{o}C for 24 h to remove the remaining solvent. The dried PLA/FR composites were conditioned at in a vacuum oven at 80 ^{o}C for 12 h to avoid the possibility of retaining residual solvent before crushing it into pieces. The crushed composites were homogenized for 10 min to obtain a fine PLA/P-ABZT granule. The homogenized PLA/P-ABZT granular composites were pressed using automatic hydraulic press following a precise pressure program where samples were deposited for 2 min on a hot plate at 180 ^{o}C and pressed for 2 min at 10 bars, followed by degassing, after which the samples were pressed again for 1 min at 15 bars. The molded samples were transferred to the cold part for final pressing for 1 min, after which the molds were removed to obtain the standard samples. Neat PLA was also dissolved in chloroform and pressed into standard samples following the same pressure program. The specimen used for the tensile test were cut into dumb-bell shaped from the films cast in petri dishes.

2.4 Characterization

ABZT, P-ABZT and the char residues were characterized by FT-IR spectrometer equipped with attenuated total reflection (ATR) accessory between 4000 - 650 cm^{-1} at 4 cm^{-1} after averaging 16 scans.

^{1}H, ^{13}C, and ^{31}P NMR spectra of P-ABZT was recorded with Bruker AV400 NMR spectrometer (Germany), using DMSO-d6 was used as solvent.

Thermal properties of ABZT, P-ABZT, and PLA/P-ABZT composites were studied with a TGA/DSC 1 Star System by Mettler Toledo between 40 - 600 ^{o}C at 20 ^{o}C/min in air with samples weight 4 - 5 mg. Mass loss profiles were analyzed as percentage mass loss with respect to temperature and the mass loss at 5% ($T_{-5\%)}$ was taken as the onset decomposition temperature whereas T_{max} denotes the temperature at which maximum decomposition occurred. TG-FTIR instrument, TGA Q5000 V3.13 Build 261 was used

to study the pyrolysis gaseous products of P-ABZT/PLA. Measurement was done from 25 to 700 °C at a heating rate of 10 °C/min in the scanning range 4000 to 450 cm^{-1} with sample weight of about 10 mg.

A Perkin Elmer DSC 800 instrument under N_2 atmosphere was used at 10 ^oC/min with samples weight 4 - 5 mg. Samples were sealed in Al pans and heated from 30 to 200 °C. The cooling and second heating scan were used were examined. The degree of crystallinity (χ_c) was calculated according to equation 1:

$$\chi_c = \frac{\Delta Hm}{\Delta Hmp(1-x)} x\ 100\% \qquad \text{(Eq. 1)}$$

where ΔH_m is the melting enthalpy of PLA and its FR composites used in this work, ΔH_{mp} (93.6 J/g) is the melting enthalpy of 100% crystalline PLA [32], and "*x"* is the weight of FR in the PLA composite.

The residual char obtained from the cone calorimeter test (CCT) was observed under various magnifications using a scanning electron microscope (TESCAN VEGA 3 LVSTD) after sputter coating with Au.

A Bay Spec 3 in 1 Nomadic Raman Microscope was used to characterize the char residues after CCT at 532 nm with integration between 4 - 17 ms.

The limiting oxygen index (LOI) of neat of PLA/P-TABZT composites and neat PLA measuring 130 × 6.5 × 3 mm^3 were evaluated according to ASTM D2863-97 with ZR-1 Intelligent Oxygen Index Analyzer. UL-94 vertical flame chamber (assembled in our laboratory) of neat PLA, PLA/P-ABZT composites with measuring 130 × 13 × 3.2 mm^3 were evaluated according to ASTM D3801 with five specimens for each composition.

Cone Calorimeter test (Fire Testing Technology Ltd., UK) was performed according to ISO 5660-1 standard with specimen dimension (100 × 100 × 3 mm^3) with two samples for each composition.

The tensile test was carried out on Instron 5566 with a ± 500 N load cell according to ASTM D882 - 12 standard at 5 mm/min with five dumb-bell shaped specimens measuring 50 × 5 × 0.31 mm^3 for each composition.

3. Results and discussion

3.1 Characterization of P-ABZT

Fourier transform infrared (FTIR) spectroscopy remains an essential analytical tool for the identification of compounds, structural elucidation, and the measurement of the fundamental properties of molecules [33]. The FTIR spectra of ABZT and P-ABZT were taken and the results shown in Fig. 1. In the spectrum of ABZT, the double narrow absorption peaks around 3480 - 3210 cm^{-1} are due to the stretching vibrations of the primary amine ($N-H_2$), which together with the aromatic ring modes give bending vibration peaks at 1660 - 1460 cm^{-1} [34]. The absorption band around 3050 cm^{-1} is assigned to C-H stretching vibrations. After modification with PPDCl, the absorption peak of the P=O bond typically appeared at 1183 cm^{-1} while the sharp peak at 946 cm^{-1} is due to the stretching vibration of P-N bond [35, 36]. The shallow absorption band of the secondary amine (N-H) stretching vibration in P-ABZT occurred around 3490 – 3263 cm^{-1} with its bending mode around 1556 $cm^{-1.}$ Also, prominent peaks belonging to the aromatic ring modes are observed around 1660 – 1550 cm^{-1}. To ascertain the structural integrity of P-ABZT, ^{1}H, ^{13}C, and ^{31}P NMR spectra were performed, and the results are shown in Figs.1 (b) and S1(a-b). From the ^{1}H NMR spectra of P-ABZT, the singlets and doublets around 6.79 - 7.0, and 7.79 - 8.09 ppm relates to the resonance vibrations of the hydrogen atoms in the aromatic ring of PPDCl, while the singlet and the multiplet around 7.46, 8.09 - 7.23 ppm relates to the resonance vibrations of the hydrogen atoms in ABZT. From the ^{13}C and ^{31}P NMR spectra of P-ABZT, the number of carbons atoms present in P-ABZT was confirmed by ^{13}C NMR with the resonance vibration of phosphorus occurring around 12.25 ppm as shown in Fig. SI (b). To determine the purity of P-ABZT, energy dispersive X-Ray spectroscopy (EDS) was conducted, and the results are shown in Fig. S2, Table S1. From the EDS map and quantitative analysis, no traces of impurity were found in P-ABZT, especially Cl. The presence of N-H and P-N absorption peaks in FTIR, in addition to ^{1}H, ^{13}C and ^{31}P NMR spectra confirmed the successful synthesis of P-ABZT.

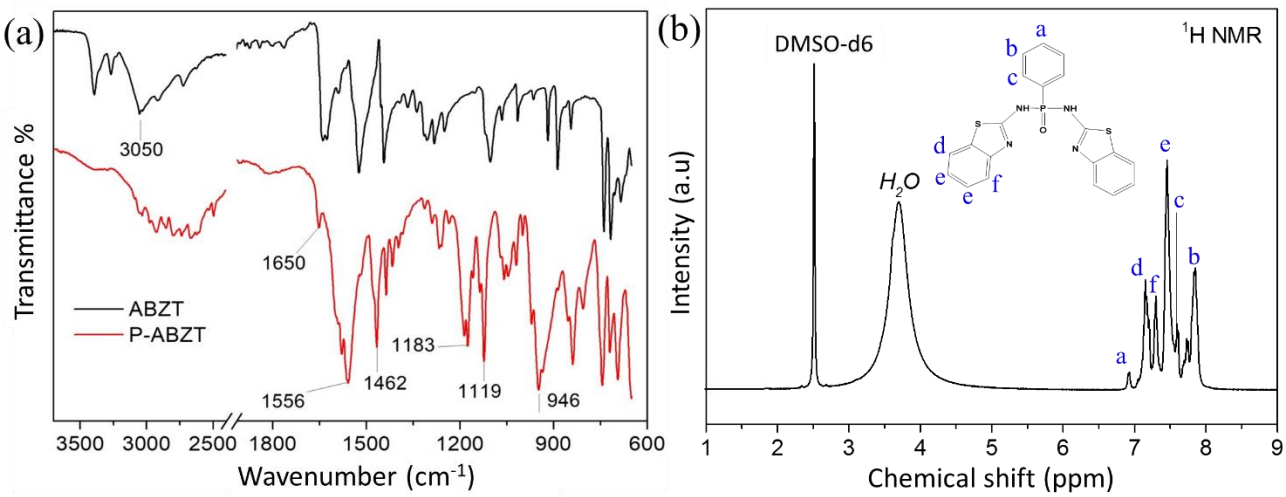

Figure 1. (a) FTIR spectra of ABZT and P-ABZT, and (b) ^{1}H NMR of P-ABZT.

3.2 Thermal properties of FR additives and PLA/P-ABZT composites

Thermal analyses of materials give insight into their thermo-physical properties, transitions, and the effect of additives on diverse production conditions [37]. To evaluate the impact of P-ABZT on the processing and final physical properties of the flame retarded PLA composites, the thermal stability of the additive (P-ABZT) was first studied, and the TGA curves are presented in Fig. 2 (a, b) with the DTG curves in Fig. S2. Table S1 summarizes the thermal characteristics extracted from the TGA and DTG curves. ABZT had three stage decompositions with a little char residue of 2.32 wt%. The initial mass loss (~ 80 wt%) happened in the range of 170 – 340 ^{o}C, with the peak at 292 °C; the second mass loss (~ 15 wt%) between 340 - 456 ^{o}C with peak at 380 ^{o}C; and the third mass loss (~ 5 wt%) between 456 – 580 ^{o}C with peak at 528 ^{o}C. The initial mass loss is attributed to the removal of crystal water still contained in P-ABZT, while the second mass loss is due to decomposition by the phosphorus, nitrogen, and sulfur groups resulting in the release of nitrogen, and sulfur oxides. The mass loss between 456-580 °C is due to the decomposition by the aromatic structures in P-ABZT and subsequent oxidation of the unstable char consequent to carbonization and final char residue. The thermal stability of ABZT improved after modification with PPDCl. This resulted in an increase in $T_{-5\%}$ and two-stage decompositions as shown in Fig. 2 (a) and Table

S1. The first mass loss (~ 30 wt%) happened in the range of 170 – 330 ^{o}C with the peak at 282 ^{o}C; second loss (~ 52 wt%) between 330 – 506 ^{o}C with a peak at 401 ^{o}C with the final residue of ~ 18 wt%. The increased thermal stability can be attributed to the presence of phosphorus, nitrogen, and sulfur in P-ABZT. Phosphorus and sulfur compounds act in both the gas and the condensed phase to reduce the degradation of polymers and promote char formation [21]. The mass loss around 401.8 °C is due to decomposition by the polyaromatic structures and subsequent oxidation of the chars resulting in carbonization with the occurrence of relatively higher char residue (Table S2). The increased char production was aided by the release of non-flammable amine gases, sulfur, and nitrogen oxides that enhanced the condensed phase mechanism of the phosphorus moiety [38, 39]. From Fig. S3 (b), a higher mass change rate (M.C.R.) (~ -2.39%) was observed for ABZT at low temperature (292.6 °C) compared to ~ -0.4% mass loss by P-ABZT at an appreciably higher temperature (401.8°C), thus confirming the thermal stability of P-ABZT.

P-ABZT was incorporated into PLA, and the results are shown in Fig. 2 (b) and Table S1. PLA had onset decomposition around 348.6 °C, leaving almost no residue at 600 °C. The $T_{-5\%}$ and $T_{max\ \%}$ of PLA reduced marginally after the addition of 0.2% P-ABZT, but a higher char residue was obtained (see Table S2). With the increase of P-ABZT in PLA, the onset decomposition temperature reduced further. The early onset decomposition is due to the early release of nitrogen and sulfur oxides. These gases catalyze cross-linking reaction between PLA and the FR radicals which reduce the burning rate and heat being generated [35]. This phenomenon results in char production which functions as a physical protective barrier that prevents the diffusion of volatile decomposition products. As shown in Fig. S3 (b), the addition of P-ABZT decreased the mass change rate (M.C.R.) of PLA from ~ -2.51 to ~ -1.5% with the 3 wt% P-ABZT loading, yielding higher char residue (see Table S2). The phosphorus species and the sulfur moiety catalyze condensation reaction in the solid phase in PLA when water is generated to promote char formation and thermal cooling.

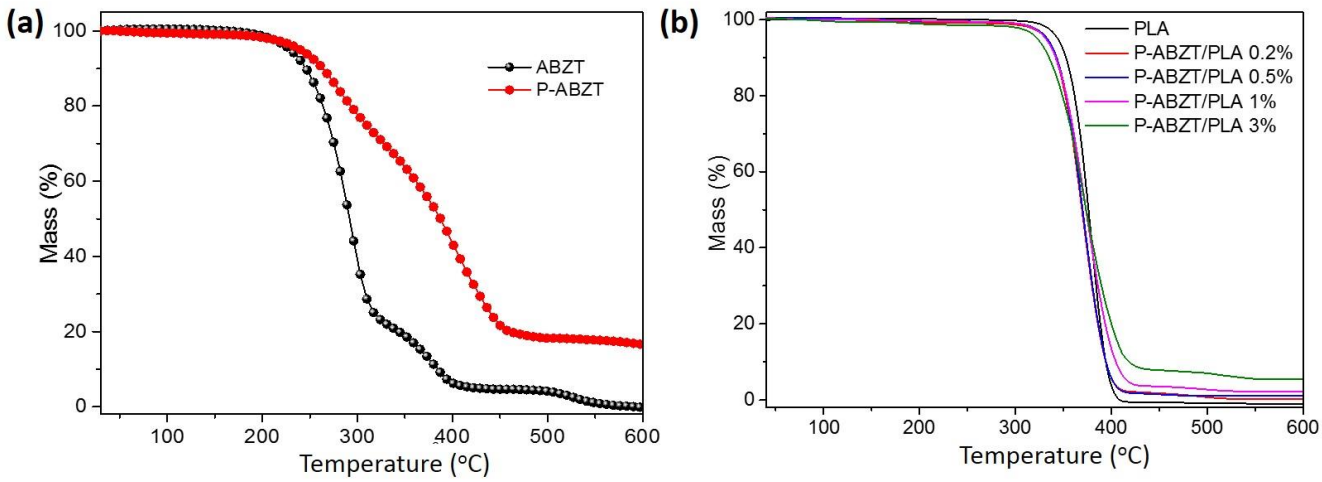

Figure 2. TGA curves of: (a) ABZT and P-ABZT, and (b) P-ABZT/PLA composites.

Crystallization plays a crucial role in the properties of semi-crystalline polymers. The DSC thermogram of PLA and its flame retarded composites obtained during the isothermal cooling and the second temperature scans are presented in Fig. 3 (a-b). The DSC data for all samples are reported in Table 1. As shown in Fig. 3 (a), pristine PLA and its composites showed no exothermic peaks in the non-isothermal cooling process from the molten state. However, an exothermic peak for PLA and the flame retarded composites are evident in the second heating scan. Typically, pristine PLA and the composites displayed unimodal endothermic peaks, indicating the absence of heterogeneous distribution of crystals [40]. The melting temperature reduced from 170.3 to 161.7 °C when the content of P-ABZT increased to 3 wt%, owing to the increase of intrinsic defect in the PLA crystals caused by the intermolecular interaction between PLA and P-ABZT [41]. The percentage crystallinity (χ_c) of neat PLA and PLA/P-ABZT composites were determined, and the results are shown in Table 1. The χ_c for PLA decreased marginally to 49.0% when 0.2 wt% P-ABZT was introduced. A further increase in the content of P-ABZT decreased the χ_c steadily to 35.9% when 3 wt% P-ABZT was added. The gradual reduction in crystallinity is due to the impedance of PLA crystal nucleation by the rigid polyaromatic P-ABZT [40, 42]. However, the Tg of

PLA/FR composites did not change significantly, indicating the inconsequential effect of P-ABZT on the amorphous segmental mobility of PLA chains.

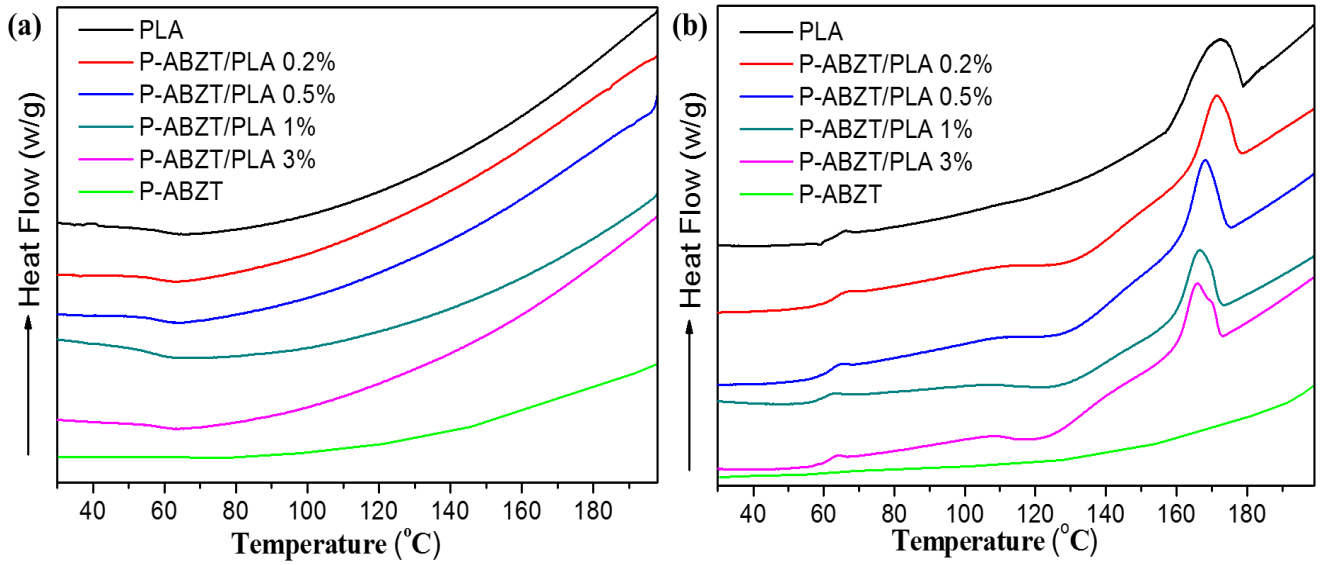

Figure 3. DSC thermogram of PLA, P-ABZT, and PLA/FR composites at a heating rate of 10 °C/min for both cooling and heating: (a) cooling curve, and (b) second heating curve.

Table 1. Calorimetry data derived from the second heating measured after cooling from the melt

Sample	T_g (°C)	T_c (°C)	ΔH_c (J/g)	T_m (°C)	ΔH_m (J/g)	X_c (%)
PLA	65.9	128.9	6.2	168.6	48.2	50.5
P-ABZT	-	-	-	-	-	-
P-ABZT/PLA 0.2%	65.5	128.8	24.9	167.9	45.5	49.0
PABZT/PLA 0.5%	65.3	130.4	30.1	170.3	42.4	45.5
P-ABZT/PLA 1%	64.8	128.8	23.0	166.4	36.4	38.9
P-ABZT/PLA 3%	64.8	123.4	35.7	161.7	32.9	35.9

3.3 Combustion behavior of PLA/P-ABZT composites

LOI and UL-94 vertical burning tests are commonly used to investigate the FR properties of polymers for specific applications. The LOI values and UL-94 results of the flame retarded PLA composites are listed in Table 2. The results show that pristine PLA is a highly flammable polymer having an LO1 of 19.8%. It did therefore not pass the UL-94 test due to relatively prolonged burning and severe melt flame dripping. The LOI of the flame retarded PLA composites increased to 22.2 % when 0.2 wt% P-ABZT was added. Meanwhile, it did not pass the V-0 rating due to melt flame dripping, although it had a shorter self-extinguishing time compared to pristine PLA. The LOI value increased further to 27.2 and 32.4% with the 1 and 3% P-ABZT loading respectively, and V-0 rating was attained with faster self-extinguishing ability (Table 2 and supplementary video file1-5). The issue of melt flame dripping was curtailed with the P-ABZT content at a quicker self-extinguishing time. The 1 wt% P-ABZT loading also extinguished almost immediately when the flame source was removed although a minimal melt dripping was observed. This phenomenon implies that the PLA/P-ABZT composites can effectively stop fire spread because the burning part will quickly drop off quickly and stop the rest of the polymer from burning. Also, fire accidents caused by melt dripping will be effectively avoided due to the absence of melt flame drips by the P-ABZT/PLA composites.

Table 2. LOI and representative UL-94 of PLA and P-ABZT/PLA composites

Sample	UL-94 Vertical test

	LOI (%)	Flame-out time (s)		Ign. of cotton	Rating
		T_1	T_2		
PLA	19.8	20 ± 2	32 ±1	Yes	N. R.
P-ABZT/PLA 0.2%	22.2	7 ±1	9 ± 1	Yes	V-2
P-ABZT/PLA 0.5%	24.8	5 ± 1	7 ± 1	No	V-2
P-ABZT/PLA 1%	27.2	1 ± 1	2 ± 1	No	V-0
P-ABZT/PLA 3%	32.4	1 ± 1	1 ± 1	No	V-0

Ign.: Ignition of cotton beneath UL-94 clamp stand

Cone calorimeter is widely used for assessing the flammability of materials at the bench scale. Samples were tested with a heat flux of 35 kW/m^2, equivalent to the average heat flux in a mild fire situation. The peak heat release rate (PHRR) and time to ignition (TTI) are essential because these parameters determine the propensity of fire ignition and propagation. These and other parameters like total heat released (THR), the average effective heat of combustion (AEHC), peak CO and CO_2 produced are presented in Fig. 4, with the detailed data summarized in Table 3. Pristine PLA exhibits strong combustion starting at ~38 s, consuming all the material with PHRR of ~ 410 kW/m^2, THR ~51 MJ/m^2, and AEHC ~17.0, leaving visibly no char. The introduction of P-ABZT at various quantities led to a decrease in PLA ignitability due to an increase in TTI as shown in Fig. 4(a). Significant reductions in PHRR (~30%), THR (~37%), and AEHC (~ 31%) were obtained with 1 wt% P-ABZT loading. When the content of P-ABZT increased to 3 wt%, the PHRR improved by ~ 50%. The significant reductions obtained can be attributed to the combined condensed and gas phase actions of the phosphorous and sulfur, in addition to the release of nitrogen oxides and ammonia gases by the primary amine in P-ABZT. The significant reductions in PHRR, THR, AEHC, and considerable delay in TTI suggest enhanced fire safety by the P-ABZT/PLA composites.

The mass loss curve of pristine PLA and the flame retarded PLA composites are shown in Fig. 4(c). Flame retarded PLA displayed early mass loss similar to the phenomenon observed in TGA analysis. The early mass loss leads to the release of ammonia gases, nitrogen and sulfur oxides that inhibits further flame propagation in the gas phase by limiting oxidations reactions. This creates incomplete combustion which leads to the formation of char in the condensed phase. The char residue serves as a physical protective barrier that insulates the underlying materials from further burning, resulting in lower PHRR and THR.

Most FRs have the undesirable effect of increasing carbon monoxide, carbon dioxide, dioxins, and hydrogen cyanide release during combustion [43]. This makes toxic fume release measurement is an essential parameter for flame retardants, because most fire deaths are caused by toxic fumes inhalation rather than direct contact with the flame itself [44]. During combustion, PLA releases mainly CO, CO_2, and water [45]. Fig. 4 (d, and S4) shows the peak CO and CO_2 produced during the entire combustion process. The CO produced for pristine and flame retarded PLA composites were high within the first 80 s with the 1 wt% P-ABZT loading having the lowest PCOP (~ 67 %). The 3 wt% P-ABZT loading led to a marginal increase in PCOP (see Fig. 4 c). The high CO peak is due to smoldering caused by delay in ignition and incomplete combustion due to the increasing content of P-ABZT. However, further reduction in PCO_2P (~ 49 %) was observed. Generally, the ratio of CO_2/CO usually indicates the combustion efficiency by revealing the degree of conversion from partial oxidization product (CO) to full oxidization product (CO_2) [46]. The results suggest that 1 wt% P-ABZT is optimal for achieving enhanced FR effect while achieving significant reductions in peak CO and CO_2 emissions. Meanwhile, the total smoke released by the composites increased with the increasing content of P-ABZT loading (Fig. S4 a). The increase in TSR can be attributed to incomplete oxidation resulting in smoldering from the flame inhibition effect of P-ABZT [47]. This phenomenon may be explained by the higher degree of secondary condensed

phase chemistry which occurs in an oxygen-depleted environment and leads to the formation of carbonaceous species.

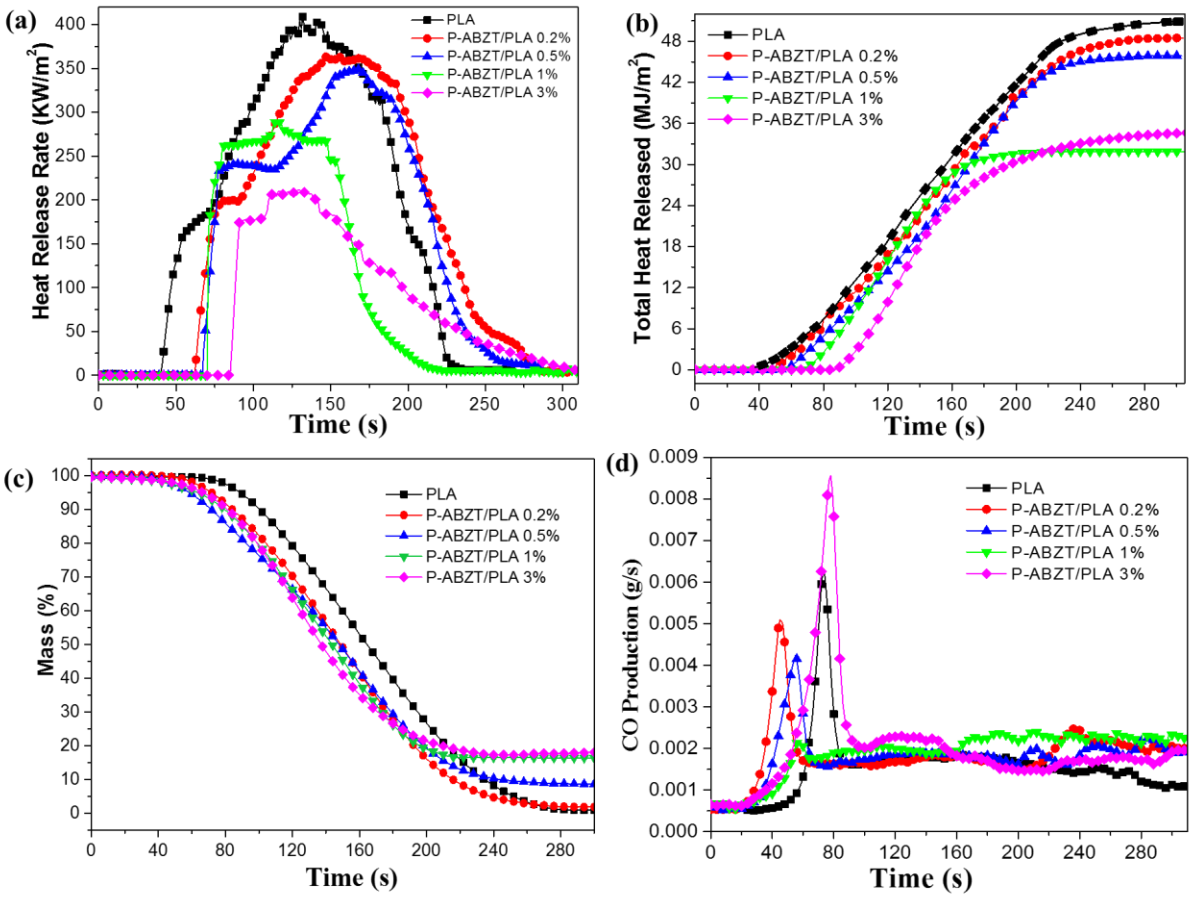

Figure 4. Cone calorimeter results of PLA and P-ABZT/PLA composites: (a) heat release rate, (b) total heat released, (c) mass loss, and (d) carbon monoxide production.

The fire performance index (FPI) of PLA/P-ABZT composites were determined, and the results are shown in Table 3. Generally, the FR performance of polymer composites relates to closely to their FPI value, such that higher FPI value denotes higher FR performance and vice versa. As shown in Table 3, the FPI of the 0.2 wt% P-ABZT loading increased from 0.1 sm^2/KW (for neat PLA) to 0.17 sm^2/KW. When the content of P-ABZT in the matrix increased further to 1wt% and 3 wt%, the FPI increased significantly to

0.24 and 0.41 sm^2/KW respectively – indicating a massive improvement in the FR performance of the PLA/FR composites. Based on the FPI values, it can be concluded that the relative time to full-blown flame flashover has improved significantly, which can allow for a safe escape for fire victims in a building.

Table 3. Cone calorimetry data for P-ABZT/PLA composites at heat flux of 35 kW/m^2

Sample	TTI (s)	PHRR (kW/m^2)	THR (MJ/m^2)	PCOP (g/s)	PCO_2P (g/s)	FPI (ms^2/KW)	AEHC (MJ/kg)	C.R (Wt %)
PLA	39 ± 3	410 ± 12	51 ± 2	0.0063 ± 0.001	0.39 ± 0.05	0.1 ± 0.01	16.9 ± 1.2	0.7 ± 0.5
P-ABZT/PLA 0.2%	61 ± 2	363 ± 7	49 ±1.1	0.0050 ± 0.006	0.36 ± 0.02	0.17 ± 0.02	16.1 ± 1	1.8 ± 0.8
P-ABZT/PLA 0.5%	67 ± 4	349 ± 13	46 ± 0.5	0.0042 ± 0.003	0.32 ± 0.04	0.19 ± 0.02	14.4 ± 1.2	8.6 ± 2
P-ABZT/PLA 1%	70 ± 4	288 ± 17	32 ± 1.2	0.0021 ± 0.002	0.27 ± 0.05	0.24 ± 0.05	11.8 ± 2	18.5 ± 3
P-ABZT/PLA 3%	85 ± 8	207 ± 15	36 ± 1.5	0.0085 ± 0.004	0.20 ± 0.02	0.41 ± 0.09	11.7 ± 4	19.5 ± 2

C.R.: Char residue, FPI: Fire performance index determined as $t_{ign}/PHRR$

3.4 Char residual analysis

The microstructure of the carbonaceous residual char after CCT gives essential information about the possible FR mechanism of composites. Digital images of char residues taken after CCT are shown in Fig. 5(a-d). A thin carbonaceous char layer possibly induced by the 0.2 wt% P-ABZT loading is observed (Fig. 5a). When the content of P-ABZT increases, a corresponding increase in char residue is observed, with

the highest char yield recorded by the 3% wt P-ABZT loading (Fig. 5 d). The SEM micrographs of P-ABZT/PLA char residues taken after CCT are shown in Fig. 5(e-h). The residual chars generally displayed a non-homogeneous aggregated microstructure, especially for the 0.2 wt% P-ABZT loading (Fig. 5 e). The 0.5 wt% P-ABZT loading shows more robustly clustered-like char morphology with cracks and less cohesive. The formation of cohesively compact char plays a vital role in achieving improved FR properties for PLA. With the increase in P-ABZT content (1 wt%), a more compact char layer is seen beneath an agglomerate particulate char. The char from 3 wt% P-ABZT loading appeared more condensed and smoother; however, tiny cracks and small fissures are observed. The tiny cracks and fissures may allow the escape of burnable gases and weaken the insulation of heat from the flame to the polymer. This phenomenon possibly contributed to the high THR and CO recorded for the 3 wt% loading in the CCT. The tiny cracks and holes in PLA/ABZT 3% composite (Fig. 5 h) can be attributed to the influence of abundant gaseous products due to the increasing amine, sulfur, nitrogen and phosphorus contents, which supports the gas phase mechanism of FR function for the composites. The char prevents direct contact between the flame and the unburnt polymer and ensures faster self-extinguishment.

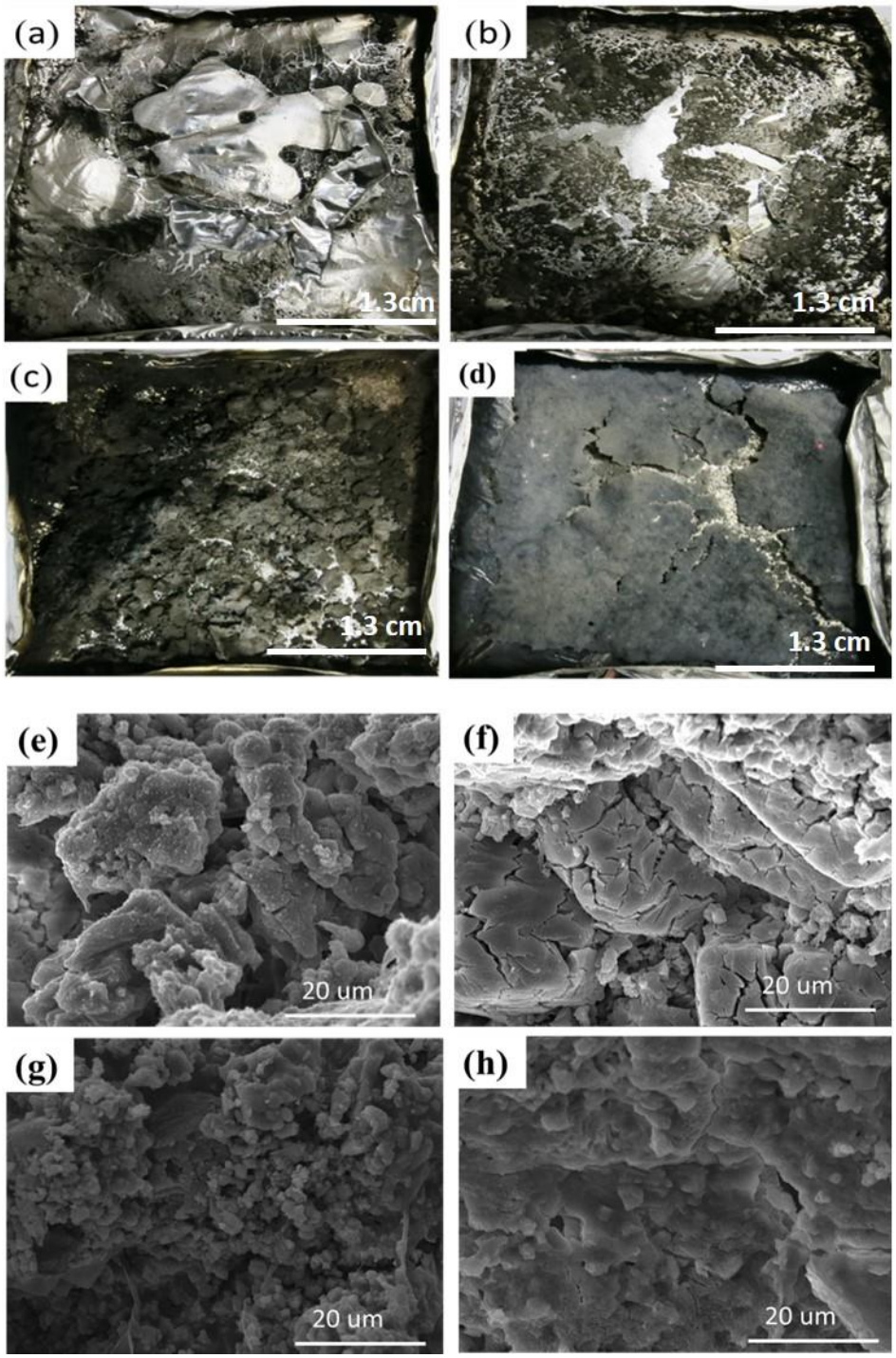

Figure 5. Digital images of P-ABZT/PLA char residues: (a) P-ABZT/PLA 0.2%, (b) P-ABZT/PLA 0.5%, (c) P-ABZT/PLA 1%, and (d) P-ABZT/PLA 3%. SEM images of P-ABZT/PLA of char residues: (e) P-ABZT/PLA 0.2%, (f) P-ABZT/PLA 0.5%, (g) P-ABZT/PLA 1%, and (h) P-ABZT/PLA 3%.

CCT char residues were further analyzed by FTIR and Raman spectra, and the results are shown in Fig. 6. The char residues displayed broad and weak absorptions around 3250 cm^{-1}, corresponding to fragments of O-H or adsorbed moisture. The tinny peak at 1652 cm^{-1} indicates the aromatic ring mode. The absorption bands at 1176 and 937 cm^{-1} are attributed to the stretching vibrations of P=O and P-N groups respectively. The intense peak at 1075, 1018, 698 cm^{-1} indicates the existence of C-O, C=S / S=O groups in chars [34] (Fig. 6 a).

To determine the extent of graphitized and amorphous carbons present in residual chars after CCT, Raman spectroscopy was used to scan the residues at 532 nm at various integration times. Fig. 6 (b) shows the Raman spectra of the char residues. The spectra typically exhibited two broad bands around 1350 cm^{-1} (D peak) and 1580 cm^{-1} (G peak), with the D peak attributed to the A_{1g} vibration mode of "unorganized carbons." The G peak is due to the presence of graphitic carbons and C=C stretching vibrations in the aromatic structures [48]. The integrated intensities (calculated as the peak area of D divided by G) of (I_D/I_G) relates to the extent of graphitization with higher I_D/I_G value indicating the presence of more amorphous chars and vice versa [49-51]. PLA/P-ABZT 0.2% had the highest I_D/I_G value (1.18) whereas that of P-ABZT 0.5% and P-ABZT 1% were 0.85 and 0.67 respectively. (See Fig. 6b). When the content of ABZT increased to 3 wt%, a further increase in I_D/I_G value (0.72) was observed. The phenomenon indicates a reduction in graphite char content. The relatively higher graphitic char in PLA/P-ABZT 0.5 and 1 wt% accounted for the improved FR effect of these composites. Also, with increases in P-ABZT loading, a shoulder peak around 1685 cm^{-1} attributed to C=N stretching vibrations in the char was observed. Another shoulder peak around 1235 cm^{-1} is ascribed to S=O asymmetric stretching vibrations of organosulfur compounds in the char because sulfur atoms exert nucleophilic attack during the burning process when water is generated [52]. An increase in the peak area of both S=O and C=N

corresponds to the increasing content of P-ABZT in the PLA matrix. From the char analysis and the results from CCT, 1 wt% P-ABZT loading is deemed optimal for obtaining a stable graphitic char layer that can protect the underlying polymer from further damage by fire and reduce toxic CO production during combustion.

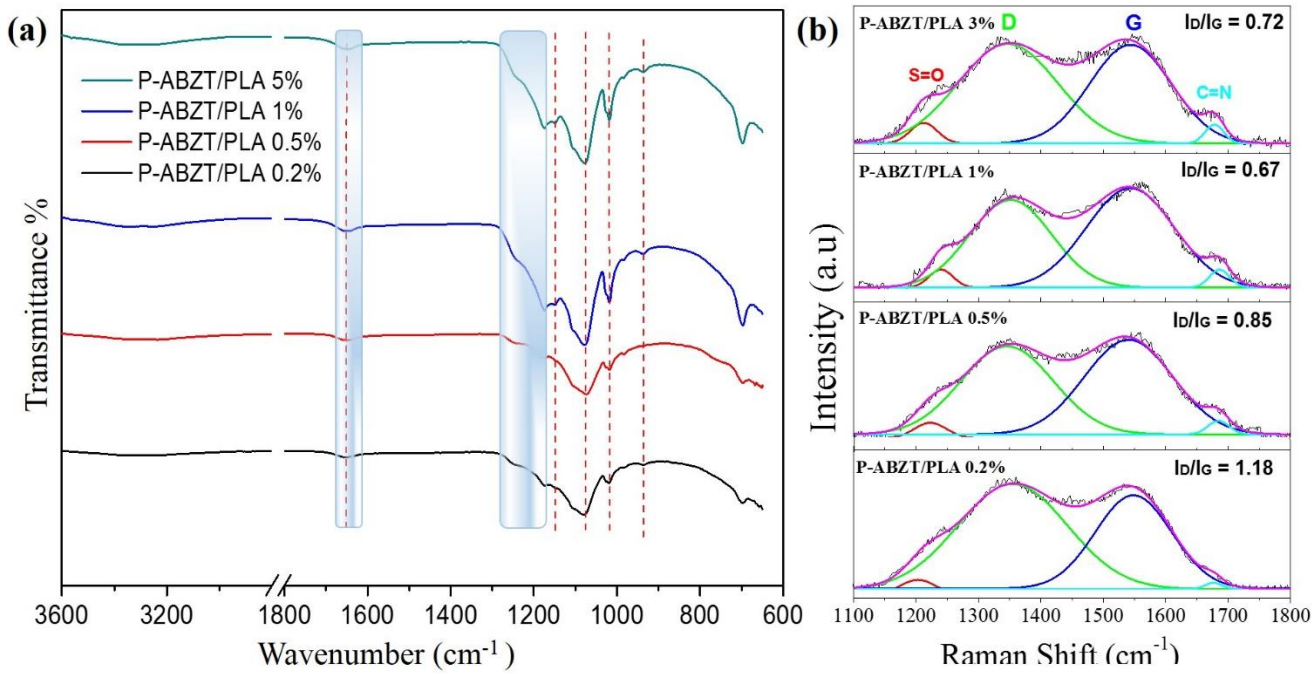

Figure 6. (a) FTIR spectra, and (b) Raman spectra of char residues after CCT.

Based on the residual char analysis, we inferred that the flame retardant mechanism of P-ABZT is based on the combined condensed and gas phase FR actions of secondary amines, nitrogen, sulfur, and phosphorus [39, 53, 54], in addition to polyaromatic nature of P-ABZT (see scheme 2). During combustion, the PLA polymer chains undergo random cessation and depolymerization in the presence of heat and oxygen leading to the production of water molecules, hydrocarbons, carbonyl compounds, aliphatic esters, CO and CO_2 [55]. At the same time, the secondary amines, nitrogen and the phosphorus components in P-ABZT break down and releases ammonia gases, non-flammable nitrogen oxides and phosphorus radicals due to its combination with the water molecules generated by PLA. The gases generated by P-

ABZT dilutes the gaseous products in the flame zone [7], and reduces the burning rate of the composite in the gas phase. The degraded phosphate group then undergoes catalytic cyclization resulting in the formation of thermally stable chars, which slows down further degradation of PLA in the condensed phase. The sulfur component contributes to the FR action mainly as a scavenger for water molecules produced during the combustion process to form sulfonic acid groups which cool down the flame and promote char formation [56]. The various functional groups and the polyaromatic structures of P-ABZT enhanced the formation of crosslinked dense char layers in the condensed phase [39], which serves as a shield on the surface of the polymer to suppress heat and mass transfer resulting in low PHRR and THR. The FR mechanism is illustrated in scheme 2.

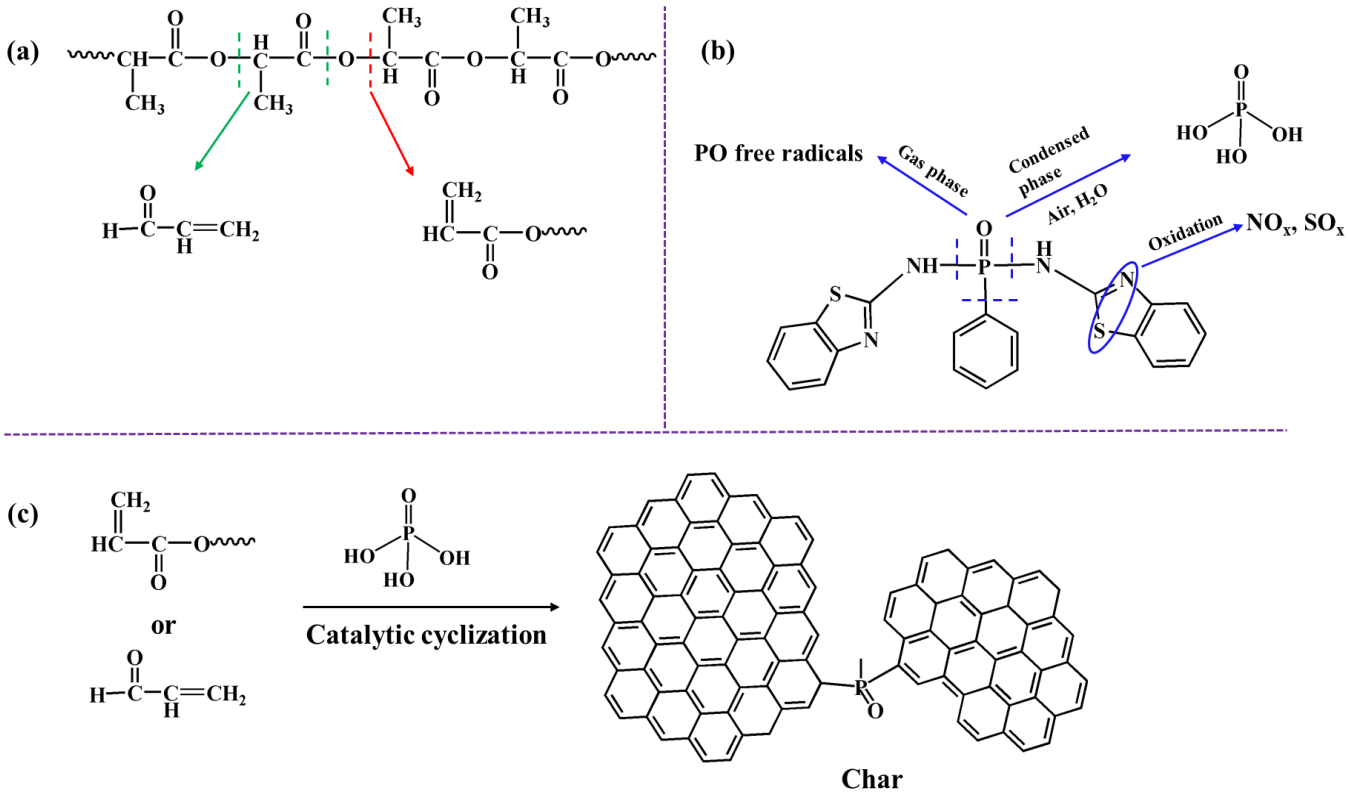

Scheme 2: Proposed FR mechanism of P-ABZT/PLA composites. Thermal decompsoition of: (a) PLA (b) P-ABZT, and (c) char formation.

3.5 Volatilized pyrolysis gaseous product analysis

The pyrolysis gaseous products evolved during the thermal degradation of neat PLA, and P-ABZT/PLA composites were examined by TG-FTIR, and the results are shown in Fig. 7. No obvious difference can be seen from the IR spectrum of neat PLA and P-ABZT/PLA composite; implying that similar volatile gases were released during the thermal degradation process. This phenomenon can also be attributed to the overlapping of weak P-ABZT/PLA composite absorbance bands by the strong pyrolysis gaseous product absorbance bands of pristine PLA. Characteristic volatilized gaseous products of PLA consisting of water, hydrocarbons, CO_2, CO, and carbonyl compounds are observed around 3506, 2900-3000, 2350, 2114-2182 and 1759 cm^{-1} respectively [57]. The absorbance around 1100-1250 cm^{-1} indicates the existence of aliphatic ester groups resulting from the PLA chain cessation during the thermal degradation process. P-ABZT/PLA recorded an overall reduction in evolved pyrolysis gaseous products compared to its neat PLA counterpart (Fig. S5). Generally, P-ABZT/PLA composites recorded significant reductions in total hydrocarbons, CO, carbonyl compounds as shown in Fig. (S5 a-d). Also, an enlarged spectrum of PLA/P-ABZT composite at maximum pyrolysis temperature showed absorption bands around 1283, 1264 and 1252 cm^{-1}, which is attributed to the evolved gaseous products of phosphorus radicals such as P=O·, P-O·, and P-OH· fragments (Fig. S6) [57].

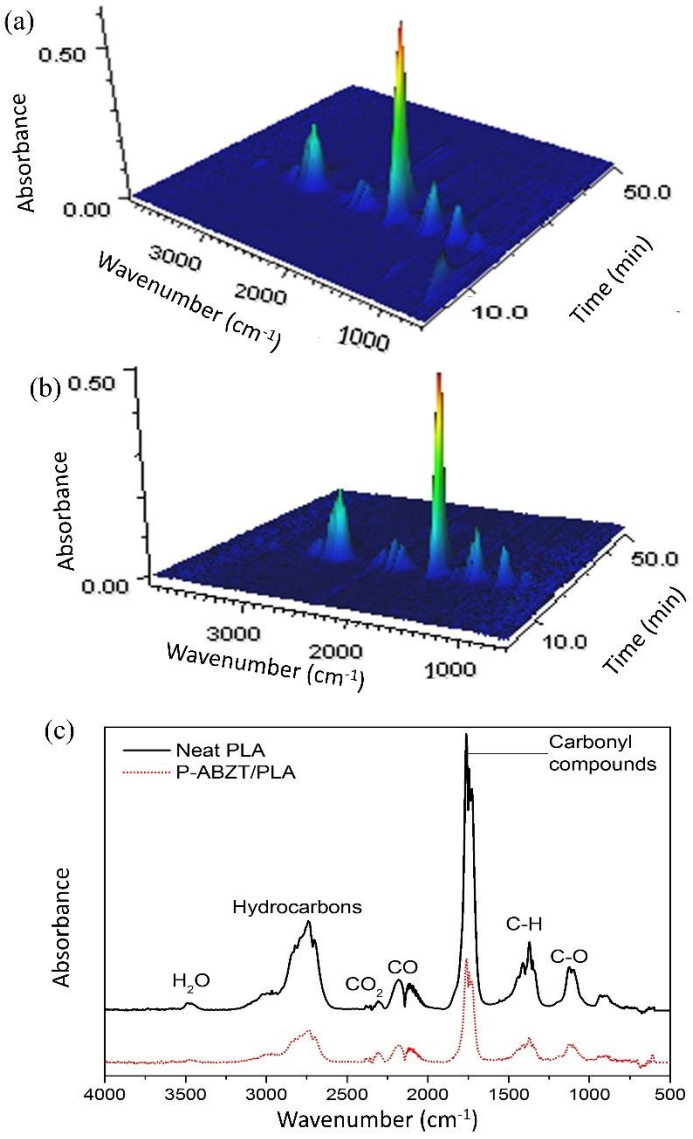

Figure 7. 3D TG-FTIR spectra of pyrolysis gaseous products of: (a) neat PLA, and (b) P-ABZT/PLA 3 wt%. FTIR absorbance spectra of pyrolysis gases from: (c) neat PLA and P-ABZT/PLA 3wt%.

3.6 Mechanical properties

The evaluation of the mechanical properties of polymeric materials is essential for the determination of their engineering end-use. The effect of P-ABZT loading on mechanical properties of PLA was evaluated, and the results are shown in Fig. 8 (a-b). Pristine PLA presents relatively high Young's modulus (~ 501.8

MPa), tensile strength (~ 54.2 MPa) and elongation at break of ~ 6.5%. Typically, 0.2 wt% PABZT loading led to a negligible increase in Young's modulus (~ 4.4%), tensile strength (~ 7.2%), and elongation at break (~ 4.6%). However, the 0.5 and 1.0 wt% P-ABZT loadings resulted in insignificant reductions in Young's modulus and tensile strength with the elongation at break remaining unchanged. As the content of P-ABZT increased to 3 wt%, a considerable decrease in tensile strength (~ 30%) and elongation at break (~ 23 %) were observed. The reduction in tensile strength and elongation at break can be attributed to the possible defects at the aggregate interface, and the increased amorphous fractions in the PLA matrix. Nonetheless, this minimal reduction in mechanical properties is still acceptable for specific applications, especially after post-stretching operations during the fiber production process [4, 31].

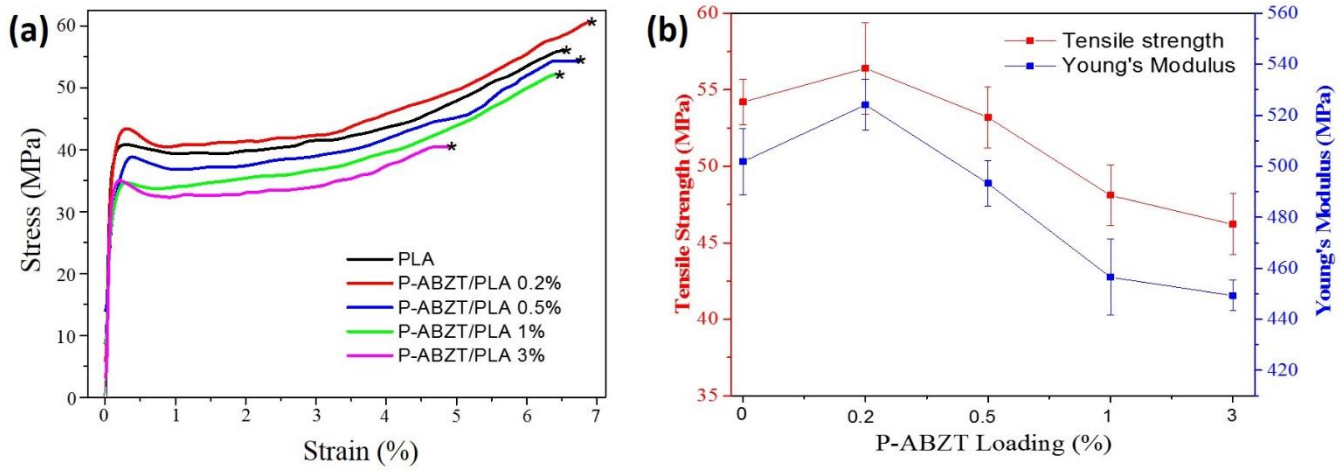

Figure 8. (a) Stress-strain curves of representative PLA and P-ABZT/PLA composites, and (b) tensile strength and Young's Modulus curves of PLA and P-ABZT/PLA of composites.

4 Conclusions

We have reported the synthesis and application of phenylphosphonic bis(2-aminobenzothiazole) (P-ABZT) flame retardant having high thermal stability and improved mechanical properties for PLA. The composite polymer was prepared by the solvent mixing and the hot compression molding approaches. The results

showed that P-BZT/PLA composites delayed the flame ignition time significantly and reduced the PHRR by ~ 50%, the THR by ~ 37%, and AEHC by ~ 31% with 3 wt% FR loading. Peak CO and CO_2 also reduced by ~ 67 and 31% respectively with 1% P-ABZT loading. Higher LOI value of 32.4% was attained with a V-0 rating in the UL-94 test. The thermal stability ABZT improved after modification with phosphorous compound (PPDCl). The improved char residue was due to the condensed phase mechanism of the phosphorus and sulfur moieties in addition to the nitrogen oxides forming a non-flammable dense char layer. DSC results showed that increasing P-ABZT content decreased and reduced the degree of crystallization in PLA as the content of P-ABZT increased to 3 wt%. TG-FTIR study demonstrated significant reductions in volatile pyrolysis products during the thermal degradation of P-ABZT/PLA composite compared to pristine PLA. The mechanical properties of pristine PLA were not compromised with 1 wt% P-ABZT loading. However, the 3 wt% P-ABZT loading led to a marginal decrease. Therefore, 1 wt% P-ABZT loading is deemed optimal for achieving acceptable flame retardancy for PLA whilst maintaining satisfactory mechanical properties.

Supporting information: Supporting information can be downloaded from doi……

Acknowledgment:
We are thankful for the funding support of GRF project 15208015. We are also grateful to Dr. Nartey Mark for language editing.

Competing Interest: The authors declare no competing financial interest in this research work.

References

[1] Tokiwa Y, Calabia BP. Biodegradability and biodegradation of poly (lactide). Applied microbiology and biotechnology. 2006;72(2):244-51.

[2] Yang W, Tawiah B, Yu C, Qian Y-F, Wang L-L, Yuen AC-Y, et al. Manufacturing, mechanical and flame retardant properties of poly(lactic acid) biocomposites based on calcium magnesium phytate and carbon nanotubes. Composites Part A: Applied Science and Manufacturing. 2018;110:227-36.
[3] Sin LT, Rahmat AR, Rahman WAWA. 1 - Overview of Poly(lactic Acid). Polylactic Acid. Oxford: William Andrew Publishing; 2013. p. 1-70.
[4] Fiori S. Industrial uses of PLA. Poly (lactic acid) Science and Technology: Processing, Properties, Additives and Applications. 2014(12):317.
[5] Madhavan Nampoothiri K, Nair NR, John RP. An overview of the recent developments in polylactide (PLA) research. Bioresource Technology. 2010;101(22):8493-501.
[6] Bourbigot S, Fontaine G. Flame retardancy of polylactide: an overview. Polymer Chemistry. 2010;1(9):1413-22.
[7] Hu XP, Li WY, Wang YZ. Synthesis and characterization of a novel nitrogen‐containing flame retardant. Journal of applied polymer science. 2004;94(4):1556-61.
[8] Shaw S. Halogenated flame retardants: do the fire safety benefits justify the risks? Reviews on environmental health. 2010;25(4):261-306.
[9] Murariu M, Bonnaud L, Yoann P, Fontaine G, Bourbigot S, Dubois P. New trends in polylactide (PLA)-based materials:“Green” PLA–Calcium sulfate (nano) composites tailored with flame retardant properties. Polymer Degradation and Stability. 2010;95(3):374-81.
[10] Kiliaris P, Papaspyrides C. Polymer/layered silicate (clay) nanocomposites: an overview of flame retardancy. Progress in Polymer Science. 2010;35(7):902-58.
[11] Tawiah B, Yu B, Fei B. Advances in Flame Retardant Poly(Lactic Acid). Polymers. 2018;10(8):876.
[12] Kovacevic Z, Bischof S, Fan M. The influence of Spartium junceum L. fibres modified with montmorrilonite nanoclay on the thermal properties of PLA biocomposites. Composites Part B: Engineering. 2015;78:122-30.
[13] Gu J-w, Zhang G-c, Dong S-l, Zhang Q-y, Kong J. Study on preparation and fire-retardant mechanism analysis of intumescent flame-retardant coatings. Surface and coatings technology. 2007;201(18):7835-41.
[14] Zhan J, Song L, Nie S, Hu Y. Combustion properties and thermal degradation behavior of polylactide with an effective intumescent flame retardant. Polymer Degradation and Stability. 2009;94(3):291-6.
[15] Tang G, Wang X, Xing W, Zhang P, Wang B, Hong N, et al. Thermal degradation and flame retardance of biobased polylactide composites based on aluminum hypophosphite. Industrial & Engineering Chemistry Research. 2012;51(37):12009-16.
[16] Wang D, Zhou K, Yang W, Xing W, Hu Y, Gong X. Surface modification of graphene with layered molybdenum disulfide and their synergistic reinforcement on reducing fire hazards of epoxy resins. Industrial & Engineering Chemistry Research. 2013;52(50):17882-90.
[17] Shi Y, Yu B, Duan L, Gui Z, Wang B, Hu Y, et al. Graphitic carbon nitride/phosphorus-rich aluminum phosphinates hybrids as smoke suppressants and flame retardants for polystyrene. Journal of Hazardous Materials. 2017;332:87-96.
[18] Wang X, Song L, Yang H, Xing W, Lu H, Hu Y. Cobalt oxide/graphene composite for highly efficient CO oxidation and its application in reducing the fire hazards of aliphatic polyesters. Journal of Materials Chemistry. 2012;22(8):3426-31.
[19] Gui H, Xu P, Hu Y, Wang J, Yang X, Bahader A, et al. Synergistic effect of graphene and an ionic liquid containing phosphonium on the thermal stability and flame retardancy of polylactide. RSC Advances. 2015;5(35):27814-22.
[20] Wang X, Song L, Yang H, Lu H, Hu Y. Synergistic effect of graphene on antidripping and fire resistance of intumescent flame retardant poly (butylene succinate) composites. Industrial & Engineering Chemistry Research. 2011;50(9):5376-83.
[21] Green J. A review of phosphorus-containing flame retardants. Journal of fire sciences. 1992;10(6):470-87.
[22] Levchik SV, Weil ED. A review of recent progress in phosphorus-based flame retardants. Journal of Fire Sciences. 2006;24(5):345-64.
[23] Mauldin TC, Zammarano M, Gilman JW, Shields JR, Boday DJ. Synthesis and characterization of isosorbide-based polyphosphonates as biobased flame-retardants. Polymer Chemistry. 2014;5(17):5139-46.

[24] Yu S, Xiang H, Zhou J, Zhu M. Preparation and characterization of fire resistant PLA fibers with phosphorus flame retardant. Fibers and Polymers. 2017;18(6):1098-105.
[25] Wei L-L, Wang D-Y, Chen H-B, Chen L, Wang X-L, Wang Y-Z. Effect of a phosphorus-containing flame retardant on the thermal properties and ease of ignition of poly(lactic acid). Polymer Degradation and Stability. 2011;96(9):1557-61.
[26] Zhao X, Guerrero FR, Llorca J, Wang D-Y. New superefficiently flame-retardant bioplastic poly (lactic acid): flammability, thermal decomposition behavior, and tensile properties. ACS Sustainable Chemistry & Engineering. 2015;4(1):202-9.
[27] Gao F, Tong L, Fang Z. Effect of a novel phosphorous–nitrogen containing intumescent flame retardant on the fire retardancy and the thermal behaviour of poly (butylene terephthalate). Polymer Degradation and Stability. 2006;91(6):1295-9.
[28] Gaan S, Sun G, Hutches K, Engelhard MH. Effect of nitrogen additives on flame retardant action of tributyl phosphate: phosphorus–nitrogen synergism. Polymer Degradation and Stability. 2008;93(1):99-108.
[29] Jian R, Wang P, Duan W, Xia L, Zheng X. A facile method to flame-retard epoxy resin with maintained mechanical properties through a novel P/N/S-containing flame retardant of tautomerization. Materials Letters. 2017;204:77-80.
[30] Schmitt TE, Sarzotti DM. Flame resistant yarns and fabrics including partially aromatic polyamide fiber and other flame resistant fibers. Google Patents; 2017.
[31] Tawiah B, Yu B, Cheung WY, Chan SY, Yang W, Fei B. Synthesis and application of synergistic azo-boron-BPA/polydopamine as efficient flame retardant for poly (lactic acid). Polymer Degradation and Stability. 2018;152:64-74.
[32] Valapa RB, Pugazhenthi G, Katiyar V. Effect of graphene content on the properties of poly (lactic acid) nanocomposites. RSC Adv. 2015;5(36):28410-23.
[33] Gaffney JS, Marley NA, Jones DE. Fourier transform infrared (FTIR) spectroscopy. Characterization of Materials. 2012.
[34] Pavia DL, Lampman GM, Kriz GS, Vyvyan JA. Introduction to spectroscopy: Cengage Learning; 2008.
[35] Liu W, Chen D-Q, Wang Y-Z, Wang D-Y, Qu M-H. Char-forming mechanism of a novel polymeric flame retardant with char agent. Polymer Degradation and Stability. 2007;92(6):1046-52.
[36] Shi X, Liao F, Ju Y, Dai X, Cao Y, Li J, et al. Improving the flame retardance and melt dripping of poly (lactic acid) with a novel polymeric flame retardant of high thermal stability. Fire and Materials. 2017;41(4):362-74.
[37] Groenewoud WM. Characterisation of polymers by thermal analysis: Elsevier; 2001.
[38] Rakotomalala M, Wagner S, Döring M. Recent developments in halogen free flame retardants for epoxy resins for electrical and electronic applications. Materials. 2010;3(8):4300-27.
[39] Green J. Mechanisms for Flame Retardancy and Smoke suppression -A Review. Journal of Fire Sciences. 1996;14(6):426-42.
[40] Krikorian V, Pochan DJ. Unusual crystallization behavior of organoclay reinforced poly (L-lactic acid) nanocomposites. Macromolecules. 2004;37(17):6480-91.
[41] Economou IG. Statistical associating fluid theory: A successful model for the calculation of thermodynamic and phase equilibrium properties of complex fluid mixtures. Industrial & engineering chemistry research. 2002;41(5):953-62.
[42] Strawhecker K, Manias E. Crystallization behavior of poly (ethylene oxide) in the presence of Na+ montmorillonite fillers. Chemistry of Materials. 2003;15(4):844-9.
[43] Stec AA, Hull TR. Assessment of the fire toxicity of building insulation materials. Energy and Buildings. 2011;43(2-3):498-506.
[44] Sheridan RL. Fire-related inhalation injury. New England journal of medicine. 2016;375(5):464-9.
[45] Costes L, Laoutid F, Brohez S, Delvosalle C, Dubois P. Phytic acid–lignin combination: A simple and efficient route for enhancing thermal and flame retardant properties of polylactide. European Polymer Journal. 2017;94:270-85.

[46] Chan SY, Si L, Lee KI, Ng PF, Chen L, Yu B, et al. A novel boron–nitrogen intumescent flame retardant coating on cotton with improved washing durability. Cellulose. 2018;25(1):843-57.
[47] Mulholland GW. Smoke production and properties. SFPE handbook of fire protection engineering. 1995;2:2.
[48] Ferrari AC, Robertson J. Interpretation of Raman spectra of disordered and amorphous carbon. Physical review B. 2000;61(20):14095.
[49] Wang G, Zhang J, Chang W, Li R, Li Y, Wang C. Structural features and gasification reactivity of biomass chars pyrolyzed in different atmospheres at high temperature. Energy. 2018;147:25-35.
[50] Yu B, Shi YQ, Yuan BH, Qiu SL, Xing WY, Hu WZ, et al. Enhanced thermal and flame retardant properties of flame-retardant-wrapped graphene/epoxy resin nanocomposites. Journal of Materials Chemistry A. 2015;3(15):8034-44.
[51] Yu B, Xing WY, Guo WW, Qiu SL, Wang X, Lo SM, et al. Thermal exfoliation of hexagonal boron nitride for effective enhancements on thermal stability, flame retardancy and smoke suppression of epoxy resin nanocomposites via sol-gel process. Journal of Materials Chemistry A. 2016;4(19):7330-40.
[52] Chen Y, Sun B, Zhang H, Zhou X. Synthesis and application of a sulfur‐containing phosphoric amide flame retardant for nylon fabric. Fire and Materials. 2016;40(7):959-72.
[53] Qian X, Song L, Hu Y, Yuen RK, Chen L, Guo Y, et al. Combustion and thermal degradation mechanism of a novel intumescent flame retardant for epoxy acrylate containing phosphorus and nitrogen. Industrial & Engineering Chemistry Research. 2011;50(4):1881-92.
[54] Granzow A. Flame retardation by phosphorus compounds. Accounts of Chemical Research. 1978;11(5):177-83.
[55] Wang X, Hu Y, Song L, Xuan S, Xing W, Bai Z, et al. Flame retardancy and thermal degradation of intumescent flame retardant poly (lactic acid)/starch biocomposites. Industrial & Engineering Chemistry Research. 2010;50(2):713-20.
[56] Zhao W, Li B, Xu M, Zhang L, Liu F, Guan L. Synthesis of a novel flame retardant containing phosphorus and sulfur and its application in polycarbonate. Polymer Engineering & Science. 2012;52(11):2327-35.
[57] Zhao P, Liu Z, Wang X, Pan Y-T, Kuehnert I, Gehde M, et al. Renewable vanillin based flame retardant for poly (lactic acid): a way to enhance flame retardancy and toughness simultaneously. RSC Adv. 2018;8(73):42189-99.

Graphic Abstract